Polymer Chemistry

Accepted Manuscript

This article can be cited before page numbers have been issued, to do this please use: T. Zhang, Z. Fang, S. Luan, L. Wang and H. Shi, *Polym. Chem.*, 2025, DOI: 10.1039/D5PY00658A.

ROYAL SOCIETY OF CHEMISTRY

rsc.li/polymers

View Article Online
DOI: 10.1039/D5PY00658A

ARTICLE

Long-Term Humid Adhesion of Sulfur Thermoplastics Polymers Enabled by Thioctic Acid-Initiated Polymerization

Received 00th January 20xx,
Accepted 00th January 20xx

DOI: 10.1039/x0xx00000x

Tongye Zhang [a, b], Zhiyue Fang [a, b], Shifang Luan[a, b], Lei Wang*[a] and Hengchong Shi*[a, b]

Inverse vulcanization shows great feasibility for the utilization and conversion of sulfur by-product into high-performance sulfur-rich polymers. However, its practical application is hindered by poorly inscrutable structural evolutions of products and thermodynamic instability. Herein, we develop a thioctic acid (TA)-initiated cascade polymerization strategy to synthesize thermoplastic polymers ($S_xT_yD_z$, where x, y, z represent the mass ratio of S_8, TA, and DIB) with controllable structural evolution and enhanced mechanical properties for humid adhesion. The key to this TA-initiated ring-opening polymerization (ROP) of sulfur is to generate S radicals at 120 °C to produce short sulfur segments and avoid the chaotic S_1D_1 networks of traditional inverse vulcanization under elevated temperature. This short sulfur structural endows $S_1T_2D_1$ with exceptional toughness (2300% of strain at breaking) and hot-pressed $S_2T_1D_1$ with reinforced strength (11.64 MPa vs. 8.5 MPa baseline). The synergy of hydrophobic sulfur and benzene motifs and carboxyl-metal coordination bonds in $S_1T_1D_1$ ensures long-term adhesion stability (>130 days) under humid environments. We believe our work establishes a platform to reconcile the trade-off between structural control and performance in sulfur polymers, offering a scalable route to repurpose industrial sulfur waste into durable adhesives for harsh environments.

1. Introduction

During the rapid development of the oil industry, sulfur is one of the main by-products of natural gas and oil refining.[1] The global annual production of sulfur is expected to reach 90 million tons in 2028, but its consumption is far from the requirements. Currently, the open-air storage and disposal of excess sulfur show various risks on its high cost and safety, and thus to lead to many environmental concerns.[2, 3] The efficient utilization of sulfur has thus garnered widespread attention due to its unique properties including the dynamic reversibility, high electrochemical capacity, and distinct optical characteristics.[4-6] Despite the great progress of sulfur-containing materials and their applications, there is still a lack of innovative strategies to harness this abundant resource effectively.[4]

As one of the most common forms of elemental sulfur (Scheme 1a), S_8 can undergo a ROP to form unstable polysulfide above 159 °C and synchronous depolymerization below this temperature in an entropy-driven and reversible manner.[7, 8] Since 2011, Pyun et al. have initiated the direct polymerizing S_8 with unsaturated olefins as cross-linking agents to synthesize sulfur-rich polymers, known as inverse vulcanization.[9] Obtained high-sulfur polymers with good solvent resistance and high electrochemical capacity can be applied into various fields, including IR imaging,[10-12] Li-S batteries,[13] and metal adsorption.[14, 15] However, sulfur-rich polymers via inverse vulcanization still face numerous challenges at elevated polymerization temperatures ($T > 170$ °C), a limited variety of vinyl monomers,[5, 16] and uncontrollable ring-opening of S_8. Additionally, the practical applications of inverse vulcanization products are restricted by several factors, including their poor mechanical properties, complex chain segment structures, and poor processability due to high crosslinking or high sulfur rank (the number of S-S units in the backbone).[17] Several strategies have proposed to solve these issues, including optimizing the ROP methods of S_8 (e.g., photoinduction,[18] ball milling[19] and organocatalysis[20-23]), adjusting polymerization processes[24, 25] (e.g., vapor-phase synthesis[26]), controlling the rigid of vinyl monomer,[27, 28] and introducing functional fillers[29] (e.g., SiO_2,[30] polyester,[31] Caron Black[32, 33] and polystyrene[34]). But the chain structure of the inverse vulcanization polymers is still unclear. Taking the typical poly(S-r-DIB) via inverse vulcanization of elemental sulfur and 1, 3-diisopropenylbenzene (DIB) as an example, it has widely been accepted that poly(S-r-DIB) has a complex cross-linked structure. But the recent work reported by Pyun et al. indicated that the predominant repeating unit in poly(S-r-DIB) consists of thiocumyl units and the previously reported "idealized" microstructures (as shown in scheme 1a).[35] Long sulfur rank polymers exhibit low modulus, poor thermal stability, while short sulfur rank polymers show poor toughness, high brittleness and processing difficulty.[5, 36, 37] Consequently, further studying underlying mechanisms and precise regulation of chain segments of inverse vulcanization remains imperative.

[a] State Key Laboratory of Polymer Science and Technology, Changchun Institute of Applied Chemistry, Chinese Academy of Sciences, Changchun 130022, P. R. China. E-mail: shihc@ciac.ac.cn, leiwang@ciac.ac.cn.
[b] School of Applied Chemistry and Engineering, University of Science and Technology of China, Hefei 230026, P. R. China.
†Electronic supplementary information (ESI) available.

View Article Online
DOI: 10.1039/D5PY00658A

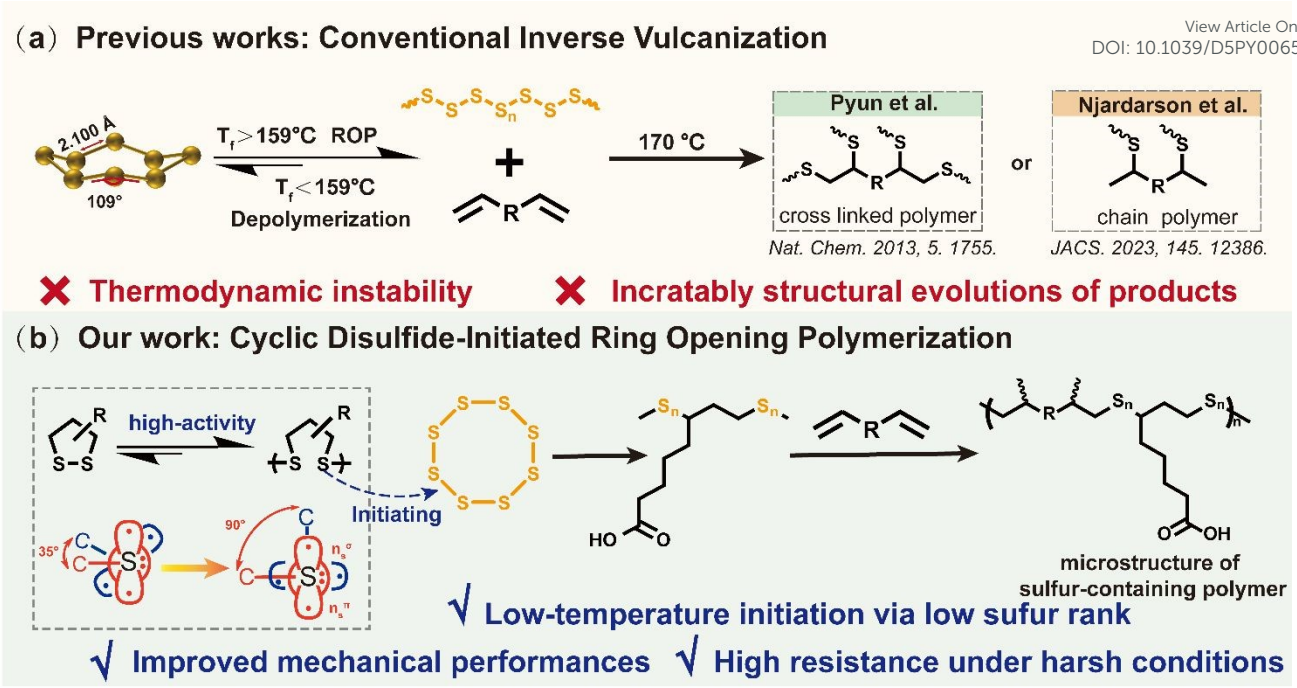

Scheme 1. Polymerization Strategies of Element Sulfur into Sulfur-Containing Polymers a) The summary of previous conventional inverse vulcanization, containing thermal-induced S_8 ring-opening polymerization and different microstructures of polymers in 2013 and 2023. b) The design of this work involves cyclic disulfide-initiated ring opening polymerization of S_8.

2. Experimental

In a 20 mL glass bottle equipped with a magnetic stirrer was added elemental sulfur (S_8, the quality detailed below) and then heated in aluminum heating blocks to 150 °C until an orange sulfur melt was obtained. Then the measured thioctic acid (TA) was appended to the glass bottle, stirring at 150 °C for 2 hours, until the molten liquid was no longer cloudy and cherry red, immediately 1, 3-diisopropenylbenzene (DIB, the quality detailed below) was dropped slowly into the bottle until the color of molten liquid became dark red and the concentration was significantly increased. Immediately, the molten liquid was poured into the 153 °C PTFE mold (preheated for 1h), stabilized for 1h, then hot annealed, and stable cured for 48 h. The sample and mold were taken out from the oven and then taken out the sample. The glass plate under the mold was leveled ahead of time to prevent uneven sample curing.

3. RESULTS AND DISCUSSION

3.1 Effect of TA Initiating S_8 Ring-opening

To clarify the influences of TA-initiating S_8 ring-opening reaction, we first studied the ROP reaction process of S_8 and TA under specific temperature conditions, monitored by using Raman and Electron paramagnetic resonance (EPR). As shown in Figures S1, S2 and Table S1, S_8 can be melted merely at 120 °C, but cannot undergo ROP even prolonging the reaction time to 12h, as proven by the unchanged Raman signal at 472 cm^{-1}. For S_8, no characteristic signal of sulfur radicals is observed when the temperature is below 120 °C, but it appears at 150 °C (Figure S3). These results indicate that S_8 cannot undergo a ring-opening reaction to generate the radical below 120 °C. But for TA, it can be completely opened and self-polymerized at 120 °C as shown in the significantly enhanced Raman of sulfur chain located at 512 cm^{-1}, attributing to the presence of asymmetric/symmetrical S-S bond (Figures S4 and S5) Both the generated sulfur radical below melting point of TA and the chemical shifts of -S-CH_2- and -S-CH- in PTA take together to confirm the successful ring-opening of TA (Figures S6 and S7).[33] Meanwhile, S radical signals of TA appeared in the EPR spectrum with a g-factor of 2.0045 under heating at 120 °C. Once S_8 powder was added into this TA system, TA gradually initiated the ROP of S_8 to produce more S radicals. And its EPR spectrum (Figure 1c) shows that the S radical signals (g = 2.0045) given a slight shift after the addition of S_8 powder, which could belong to the S radicals after TA-induced S_8 ring-opening and copolymerization.[21, 55] We also recorded the phase changes of the above reaction processes using digital photos. After the complete melted mixture of S_8 powder and TA, an obvious phase separation was observed due to the great difference in polarity. With the increasing heating, the molten liquid of S_8 and TA transitions from a yellow and flowing state to a brown and viscous state (Figure 1e and Table S2).[56] We regularly extracted the molten liquid of S_8 and TA for Raman tests at regular intervals. As shown in Figure 1d, the observed asymmetric/symmetric S-S bond stretching vibration of TA at 512 cm^{-1} shifts to the vibration of the deformed/stretched -S-S_X-S- vibrations at 473 cm^{-1}, suggesting the successful ROP of S_8.[22, 57] Therefore, we can conclude that TA first undergoes ring-opening and self-polymerization at 120 °C. The terminal sulfur radicals of the ring-opening of TA and PTA remain active and can serve as initiators for sulfur ring-opening. Finally, the sulfur

View Article Online
DOI: 10.1039/D5PY00658A

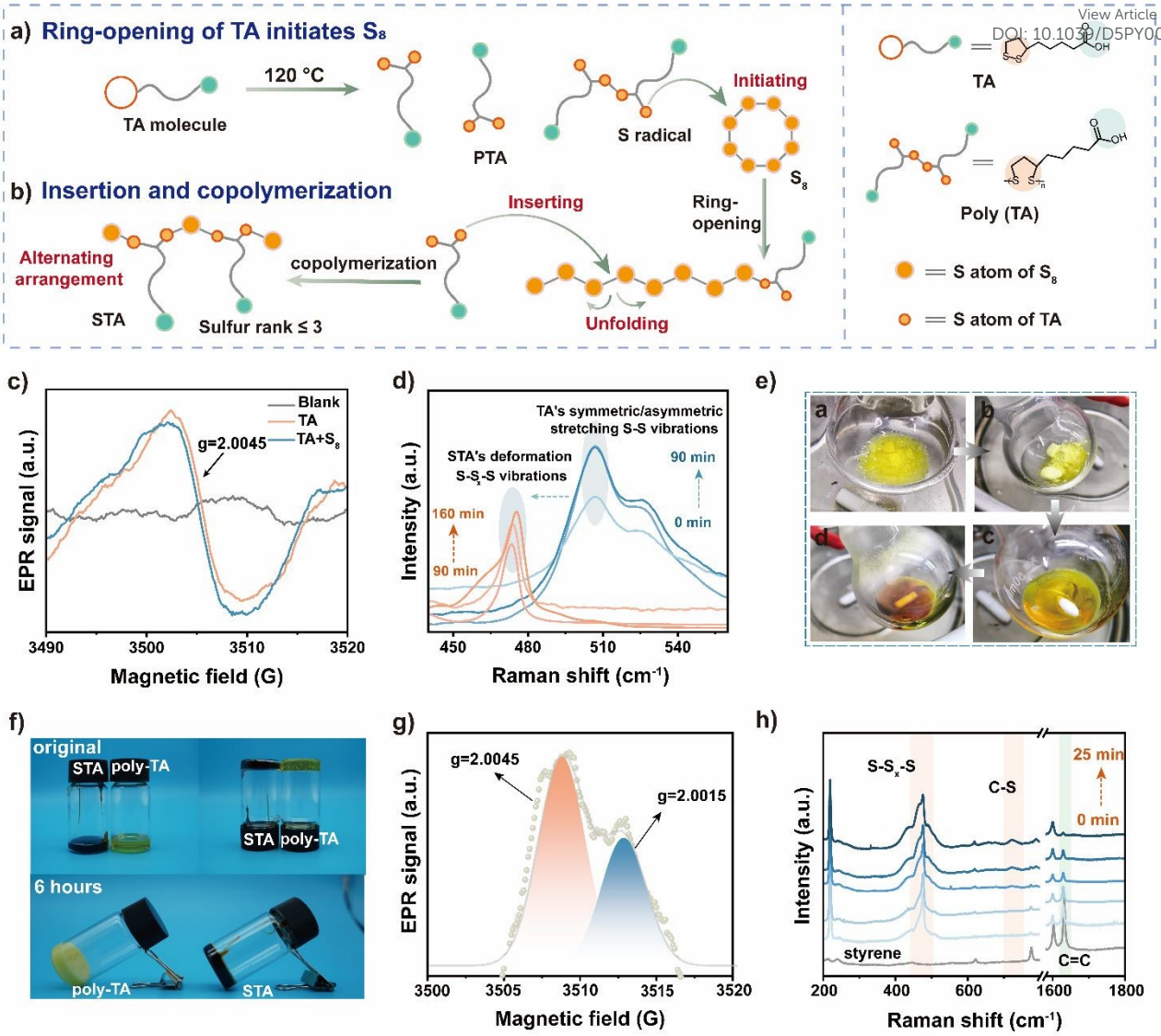

Figure 1 TA-initiated ring opening polymerization of inverse vulcanization polymers. a) Process of ring-opening of TA initiates S_8. b) Insertion and copolymerization of PTA and S_8. c) EPR spectra of TA and the mixture of TA and S_8. d) Raman spectra of TA and the STA at variable times. e) Pictures of the changes in PTA and STA at room temperature. f) EPR spectra of STA and styrene, with corresponding S and C radicals accompanied by associated curve fits. g) Raman spectra of the STA and styrene mixture at variable times. h) Reaction characteristics of the ter-polymerization of S_8 with TA and reactivity in DIB addition.

radicals of TA or PTA successfully initiate the eight-membered ring opening of S_8 powder at 120 °C (Figure 1a).

3.2 Role of TA in Regulating Chain Segments in Inverse Vulcanization

Subsequently, we studied the effect of TA in regulating the chain segments in inverse vulcanization by various model reactions (Scheme S1-3), including the polymer of poly (S_8-TA) (named STA), poly (S_8-TA-styrene) and poly (S_8-styrene). Among poly-S_8, PTA and STA polymers, it is more interesting that the copolymer of STA can be maintained at room temperature for more than six hours, while PTA begins to crystallize and precipitate within 10 minutes, even poly-S_8 begins to depolymerize below 159 °C (Figures 1f and S8). This can be attributed to the mutual stabilizing effect of the copolymer of S_8 and TA. Then we reacted styrene with STA prepolymer at 120 °C and monitored the reaction process. EPR shows the signals of C radical (g = 2.0015) and S radical (g = 2.0045), and the Raman shows the disappearance of the double bond peak at 1628 cm^{-1}. These findings indicate the successful addition of styrene during the reaction. And the formation of -S-S_X-S- and C-S demonstrates the successful synthesis of poly (S_8-TA-styrene) (Figures 1g and 1h).

3.3 Structural analysis of Poly (S_8-TA), Poly (S_8-TA-styrne) and Poly (S_8-styrene)

After that, we conducted an in-depth structural analysis of poly (S_8-TA), poly (S_8-TA-styrene) and poly (S_8-styrene) by electrospray ionization mass spectrometry (ESI-MS). These three products could have different sulfur segments via structural control. ESI-MS confirms that the highest sulfur rank can be identified as 3 for molecular weight less than 400 in mass spectrometry of poly (S_8-styrene) (Figure S9a). However, the highest sulfur rank in poly (S_8 - styrene) can be calculated to be more than 10 when the molecular weight exceeds 600 (Figure S9b). The inherent instability and extensive cross-linking within

View Article Online
DOI: 10.1039/D5PY00684A

the polymer could give great challenges in precise structural elucidations. This aligns with previous studies highlighting the uncontrollable nature of the ring-opening polymerization (ROP) of S_8 in conventional inverse vulcanization systems, which typically generate disordered, elongated sulfur chain architectures.[36, 37] But for STA and poly (S_8-TA-styrene), the sulfur chain segment has significantly decreased. As shown in Figure S10, we can observe the signal peaks that reflect the structural characteristics of the polymer chain in the mass spectrum of STA. The highest sulfur rank in the STA is calculated to be 5. We proposed that the chemical reactivity of the sulfur chain was significantly enhanced after the TA initiated ROP of S_8. Under such circumstances, the S radical generated by TA can smoothly insert into the long sulfur chain and form a unique structure with alternating TA and S atoms. The insertion behavior of TA may limit the continuous growth of the sulfur chain, which is beneficial to obtain many short sulfur chain segments with good stability. Subsequently, we further investigated the structure of poly (S_8-TA-styrene). As shown in the mass spectrum of poly (S_8-TA-styrene) (Figure S11), the molecular weight of the poly (S_8-TA-styrene) polymer model is also highly consistent with the experimental data, and the determined sulfur rank is about 4 or 5. Obviously, this short sulfur rank in poly (S_8-TA-styrene) than other samples may lead to enhanced structural stability. Moreover, it also indicates that the incorporation of unsaturated styrene monomers does not affect the chain segment regulation of TA on S_8. Thus, a series of poly (S_8-TA-styrene) products with short sulfur rank are obtained by TA regulating the segment of poly (S_8-styrene). Detailed structural factors in Tables S3-5 exhibit the observed m/z values with proposed structures, accounting for sulfur chain length. Finally, the reaction kinetics of STA and poly (S_8-TA-DIB) were studied in detail by monitoring the conversion of TA and DIB as well as the corresponding changes in molecular weight during the polymerization reaction via ^{1}H NMR and GPC traces (Figure S12-20).[58] After the co-polymerization of S_8 with TA, the molecular weight of STA does not increase significantly with the increase of TA conversion rate, indicating the sulfur rank number below five is maintained well. After adding DIB, the molecular weight of poly (S_8-TA-DIB) increases promptly due to the possible formation of cross-linking sites (Figure 1h). These results indicate that the introduction of TA could transform the long sulfur chain structures into shorter sulfur chain segments with fewer than five sulfur atoms. It is established that TA functions dually to both initiate sulfur ring-opening at 120 °C and mediate chain segment regulation through terminal sulfur radicals, resulting in structurally stabilized short sulfur rank polymers.

3.4 Structural and Chain Segment Regulation by TA Characterizations

After elucidating the TA-initiated chain segment regulation, we synthesized a series of poly (S_8-TA-DIB), named $S_XT_YD_Z$ (where x, y, and z represent the mass ratios of S_8, TA, and DIB in the ter-polymerization), including $S_2T_1D_1$, $S_1T_1D_1$, and $S_1T_2D_1$. The subsequent structural analysis takes $S_1T_1D_1$ as an example and uses it as the representative of the experimental group. As shown in Figure 2a, the obtained Raman spectrum of $S_1T_1D_1$

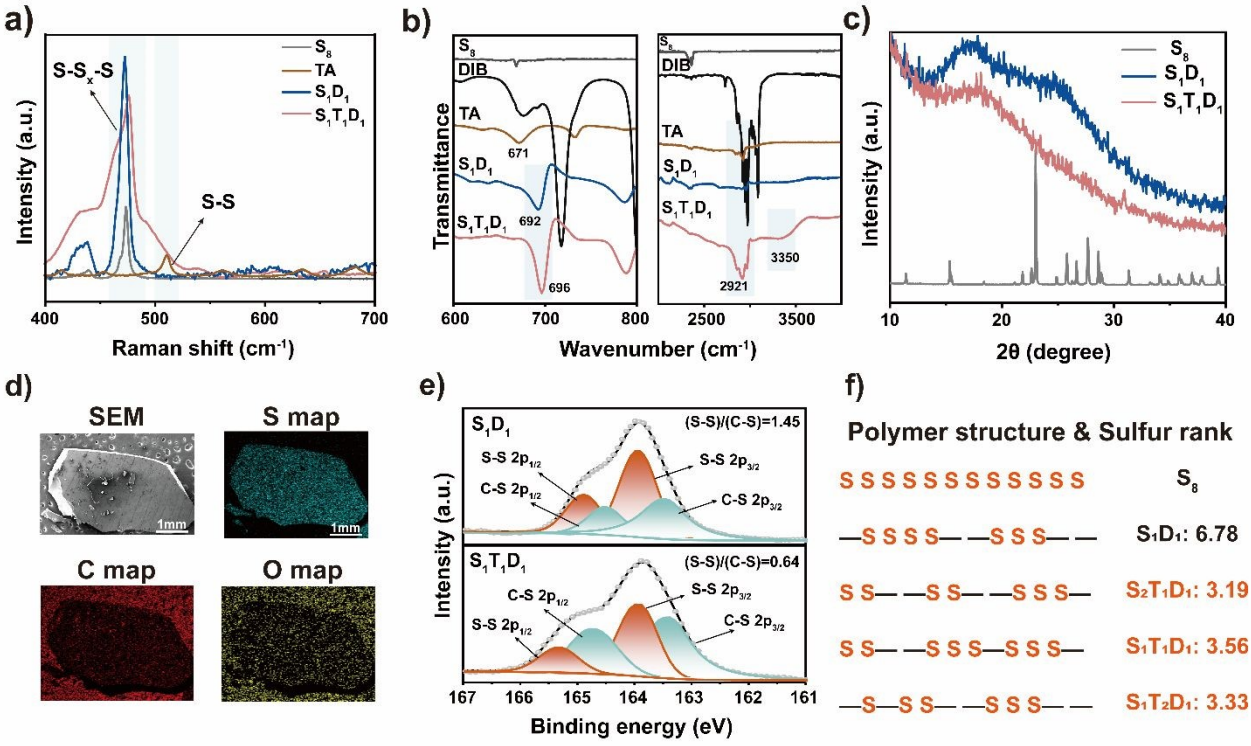

Figure 2 Structure characterizations and sulfur rank of $S_XT_YD_Z$. a) Raman spectra of the control S_1D_1 and $S_1T_1D_1$ containing the monomers of TA and S_8. b) ATR FT-IR spectra of the control S_1D_1 and $S_1T_1D_1$ containing the monomers of S_8, DIB and TA. c) XRD patterns of the control S_1D_1 and $S_1T_1D_1$ compared to the elemental sulfur. d) SEM images of the $S_1T_1D_1$ and its corresponding elemental mapping displayed on the right side. e) X-ray photoelectron spectra of the control S_1D_1 and $S_1T_1D_1$. f) Cartoon illustration of the internal structure of control S_1D_1 and $S_XT_YD_Z$ with different ratios, "—" stands for carbon-carbon bond and sulfur rank obtained by elemental analysis.

View Article Online
DOI: 10.1039/D5PY00658A

sample in comparison with its S_8, TA, and S_1T_1 controls reveals a significant structural transformation as proven in the disappearance of the disulfide bond peak at 510 cm^{-1} for the TA monomer and the emergence of a new -S-S_X-S- peak at 470 cm^{-1}.[22, 57] These observation confirms the successful ring-opening of TA and its induced copolymerization with S_8 to form polysulfide chains.[22] Meanwhile, as shown in the Fourier-transform infrared spectroscopy (FT-IR) (Figure 2b), $S_1T_1D_1$ exhibits the same C-S bond peak at 696 cm^{-1} as that of the S_1D_1 sample. And an obvious wavenumber shift is observed from the C-S bond peak at 671 cm^{-1} in TA to the C-S bond peak at 696 cm^{-1} in $S_1T_1D_1$. This shift in $S_1T_1D_1$ can be attributed to the increased polarity arising from electron-withdrawing groups on the benzene rings within the $S_1T_1D_1$ polymer structure, and the lone pair electrons on the sulfur atoms can form a weak conjugation system with the benzene rings. Meanwhile, the peak corresponding to wavenumber around 3350 cm^{-1} can be attributed to the stretching vibration absorption peak of O-H bonds of carboxyl groups, which indicates the presence of hydrogen bonding between the $S_XT_YD_Z$ polymer chains and the enhanced vibration peak of the carboxyl group (1681 cm^{-1}) was enhanced with the increase of content of TA (Figures 2b, S21).[59, 60] The appearance of the carbonyl carbon peak at 180 ppm in the ^{13}C solid-state NMR and C-H assignment in the ^{13}C-^{1}H HMQC spectrum of $S_1T_1D_1$ also confirm the ter-polymerization result (Figures S22-25). Compared with DIB, the disappearance of C=C stretching vibration absorption at 1634 cm^{-1} and CH- stretching vibration at 3087 cm^{-1} in S_1D_1 and $S_1T_1D_1$ significantly demonstrate the consumption of C=C bonds and allylic hydrogens (Figure S26).[61] These results demonstrate the successful adduction of DIB. We performed X-ray diffraction (XRD) analysis on the $S_1T_1D_1$ sample and its S_8, S_1D_1 control. A broad peak located near 18° suggests that no elemental sulfur exists in as-synthesized amorphous S_1D_1 and $S_1T_1D_1$ (Figure 2c). The uniform distribution of C, O, and S in $S_1T_1D_1$ was confirmed in scanning electron microscopy (SEM) images (Figure 2d), suggesting the homogeneous reaction of S_8, TA, and DIB monomers.

We further explicated the segmental structures of $S_XT_YD_Z$ through X-ray photoelectron spectroscopy (XPS) and elemental analysis (EA). Both XPS and EA tests confirm a significant reduction in sulfur content after incorporating TA, indicating the successful synthesis of short sulfur rank polymers. The bond structure and sulfur content of S_1D_1 and $S_XT_YD_Z$ were first analyzed by XPS. As shown in Figure 2e and Table S6, the XPS results for $S_1T_1D_1$ reveal that the S2p peak consists of two different chemical environments at 163.48 and 164.88 eV for C-S bonds as well as 163.98 and 165.38 eV for S-S bonds, respectively. The sulfur rank calculation is based on peak deconvolution of S-S and C-S on XPS data. And the final ratio of S-S to C-S in $S_1T_1D_1$ polymer is calculated to be 0.64, indicating that the average sulfur rank in the $S_1T_1D_1$ chain segments is approximately 3.56. The obtained sulfur rank of S_1D_1 control is calculated to be 6.78 (Figures S27-28 and Table S7). Notably, the sulfur rank of $S_XT_YD_Z$ decreases from 6.78 to 3.56 after the introduction of TA. The sulfur content of $S_XT_YD_Z$ shows discrepancies between XPS and theoretical feed ratios, ranging from 11.58 to 67.13 wt% % (Table S8). Taking $S_1T_1D_1$ as an example, the sulfur content detected by XPS for the same polymer is 20.85 and 35.07 wt% %, showing a large discrepancy. But for the results from EA (Table S9), it provides a closer value of 41.966 and 43.443 wt% % for $S_2T_1D_1$. Considering the limitations of the XPS test, such as surface sensitivity and semi-quantification, the sulfur rank based on the sulfur content results from EA is more convincing.

According to previous works,[62, 63] the sulfur contents obtained for the control S_1D_1 and $S_XT_YD_Z$ via EA can be further divided into two parts, including sulfur incorporated into the polymer backbone as well as sulfur not incorporated into the polymer backbone. And the latter has been defined to be “dark sulfur” by Tom Hasell. This so-called “dark sulfur” is distributed in the polymer matrix in an amorphous form and is regarded as an interference in the accurate calculation of the sulfur rank. Ultraviolet–visible spectrum (UV-Vis) was performed to test the content of dark sulfur. By establishing a standard curve based on the Beer-Lambert plot curve, the corresponding “dark sulfur” content in each as-synthesized polymer can be calculated to be 5.258wt % for control S_1D_1, 4.091wt % for $S_2T_1D_1$, 6.517wt % for $S_1T_1D_1$, and 9.432wt % for $S_1T_2D_1$ as listed in Table S10, respectively (Figures S29-30 and Table S9).[62, 63] Following that, the remained polymerized sulfur contents after excluding the contributions of “dark sulfur” are calculated and listed in Table S9. As shown in Table S10, the average sulfur rank in $S_XT_YD_Z$ and its control S_1D_1 is calculated by EA and XPS, and the corresponding results can be compared directly. Both EA data and XPS data exhibit a consistent decreasing trend with the increasing TA content. Obviously, due to semi - quantitative nature of XPS calculation, the sulfur content calculated by EA has smaller errors. For data from EA, the sulfur rank significantly decreases from 9.95 for S_1D_1 without adding TA to a minimum of 3.02 for $S_1T_2D_1$ at the highest TA amounts. This reduction in the number of sulfur rank shows a shortening of the sulfur chain length within the segment of the polymer, indicating the successful regulation of the polysulfide polymer segments by TA. The probable correlations between sulfur rank and polymer structure are proposed as shown in Figure 2f, demonstrating that TA played a critical role in regulating the chain segments in the inverse vulcanization polymers.

3.5 Thermal, Mechanical Properties and Recycling Enhancement

Excessive sulfur chain length can lead to detrimental impacts in polymer performance, manifesting as reduced mechanical properties, altered thermal stability and optical properties, increased processing difficulty, and diminished chemical resistance.[6, 37] As disscused, TA modification of inverse vulcanization (control S_1D_1) effectively suppresses the growth of sulfur rank, influencing the thermal and mechanical properties of $S_XT_YD_Z$.[64, 65] As shown in Figures 3a, S31-33 and Table S11, the decomposition temperature of the $S_XT_YD_Z$ polymer is approximately 215 °C, which is 40 °C lower than that of S_1D_1. Additionally, the differential scanning calorimetry (DSC) curves

View Article Online
DOI: 10.1039/D5PY00658A

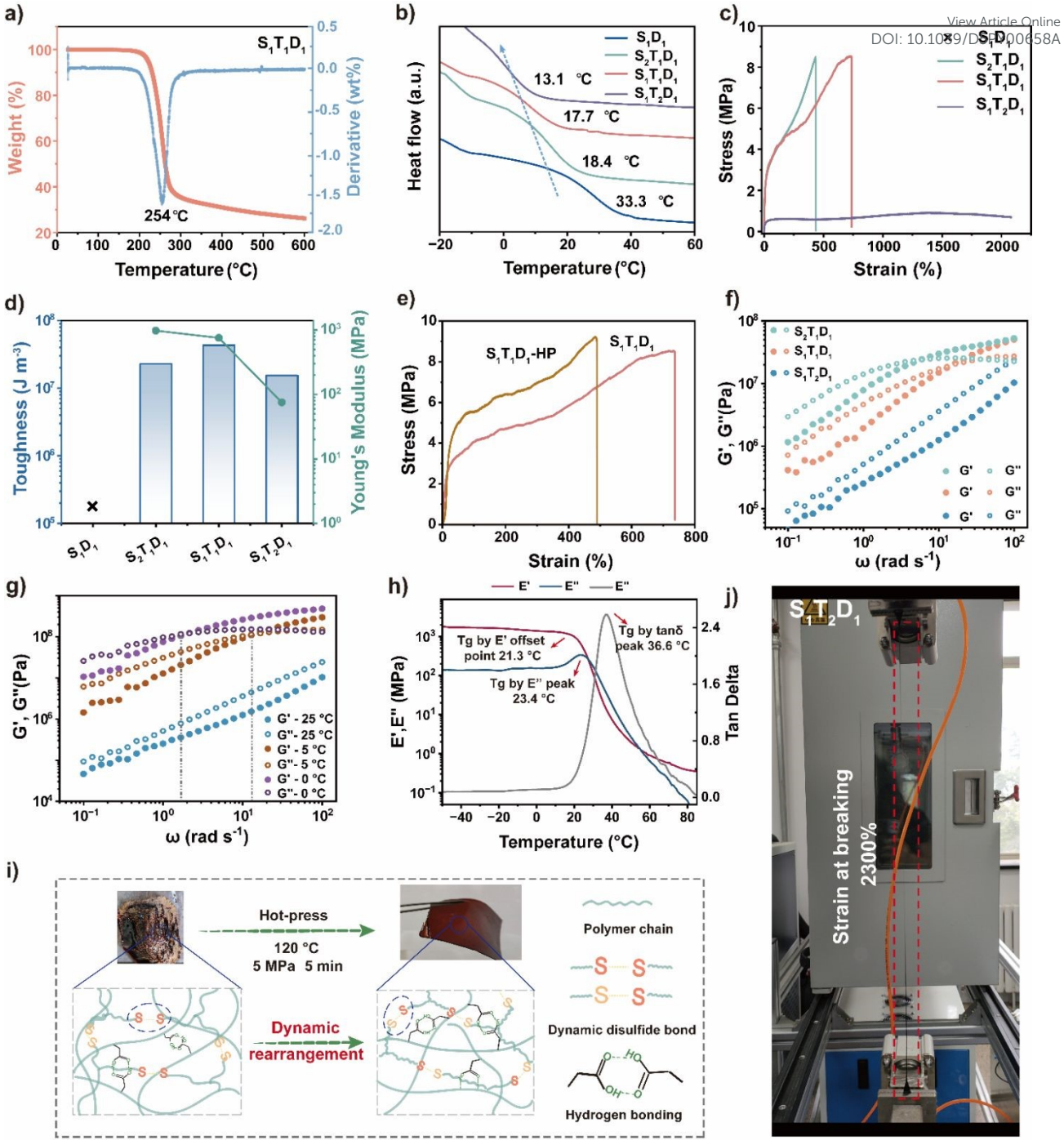

Figure 3 Mechanical and thermal properties of $S_XT_YD_Z$. a) TG curves of $S_1T_1D_1$, b) DSC curves of $S_XT_YD_Z$ and its control S_1D_1. c) Standard stress-strain curves, and d) Toughness and Young's modulus of $S_XT_YD_Z$ and its control S_1D_1. e) The stress-strain curve of $S_1T_1D_1$ after recycling. f) Rheological monitoring of $S_XT_YD_Z$ at 25 °C in the frequency sweep. g) Rheological monitoring of $S_1T_2D_1$ at 25 °C, 5 °C and 0 °C in the frequency sweep. h) Dynamic mechanical analysis of $S_1T_1D_1$. i) Diagram illustrating the dynamic rearrangement of disulfide bonds of $S_XT_YD_Z$ during hot pressing. j) The image during tensile test of $S_1T_2D_1$.

reveal that as the content of TA copolymer increases, the glass-transition temperature (Tg) gradually decreases (Figures 3b and S34). This is attributed to PTA acting as a soft segment in the $S_XT_YD_Z$, reducing the rigidity of the polymer, thereby enhancing the flexibility of the $S_XT_YD_Z$. Hot pressing is a polymer processing technique that is commonly used as a method for recycling sulfur-containing polymers. The hot-pressing process can facilitate the rearrangement of disulfide bonds within the $S_XT_YD_Z$, resulting in the formation of a dense and uniform polymer film for investigating the mechanical properties. The stress-strain curve of $S_1T_1D_1$ with S_8: TA ratio at 1:1 indicates a maximum breaking strength of 8.5 MPa, a breaking strain of 743% and a Young's modulus of 973 MPa. With the increase of TA content (S_8: TA ratio at 1:2), an ultra-high strain of 2300% is achieved in $S_1T_2D_1$ sample, but the breaking strength decreases to 1.5 MPa in comparison with $S_1T_1D_1$ sample (Figures 3c, 3d, 3j and Table S12). This is due to PTA inserts into the control S_1D_1 polysulfide chain, preventing severe chain entanglement within the $S_XT_YD_Z$. Under external stretching force, dynamic bonds in $S_XT_YD_Z$ can rapidly align and dissipate stress, thereby enabling the $S_XT_YD_Z$ to

View Article Online
DOI: 10.1039/D5PY00658A

achieve high strength and high elongation. The above results can be ascribed to the incorporation of the flexible chain, TA, increasing the distance between polymer chains, reducing the rigidity of S_1D_1 control and enhancing the flexibility of $S_XT_YD_Z$. For the inverse vulcanization polymer of S_1D_1 control both before and after hot pressing, it exhibits high brittleness due to its high degree of crosslinking, making it difficult to process and cannot to test its mechanical properties. In contrast, $S_XT_YD_Z$ polymers modified with TA show good processability. The $S_XT_YD_Z$ polymers contain a significant number of S-S bonds exhibiting short sulfur rank, which is beneficial to the reprocessing. We then hot-pressed the crushed $S_XT_YD_Z$ at 90 °C under a pressure of 5 MPa for 10 minutes to obtain a uniform polymer ($S_XT_YD_Z$ – RE), as the temperature of active disulfide bonds of the linear polymer is approximately 50-90 °C.[66] After conducting stress-strain tests on the polymer $S_XT_YD_Z$ and $S_XT_YD_Z$ - RE, we found that the breaking strength significantly increased after repeated hot pressing (Figures 3e and S36). Among them, $S_2T_1D_1$ shows the most significant increase in tensile strength, rising from 8.47 MPa to 11.66 MPa (Figure S35). To investigate the mechanisms of internal structural change during the hot-pressing process, we conducted in-situ EPR tests on the polymer $S_1T_1D_1$ during hot pressing via monitoring the generation of S radical signals (Figure S37). We observed a prominent signal of sulfur radicals during the hot-pressing process of the $S_1T_1D_1$, indicating the cleavage of disulfide bonds. As a result, this increase of breaking strength can be ascribed to the heat-initiated conditions causing the disulfide bonds in the $S_XT_YD_Z$ to break and rearrange continuously.[55] The solubility tests of the $S_XT_YD_Z$ and $S_XT_YD_Z$-HP also show that the solubility decreases significantly, and the crosslinking density increases after hot pressing (Figure S38). This process enhances inter-chain interactions, thereby leading to improved mechanical properties. We also examined the XPS spectra of the $S_XT_YD_Z$ after hot pressing and its sulfur rank remained less than 3 (Figures S39-42 and Table S7).

To investigate the flow characteristic of $S_XT_YD_Z$, we performed dynamic rheological characterizations on $S_XT_YD_Z$. As shown in Figure 3f, frequency sweep tests of $S_2T_1D_1$ and $S_1T_1D_1$ at 25 °C reveal a crossover point between storage modulus (G') and loss modulus (G"). At long timescales of low frequencies, a plateau of G' is lower than G", showing viscous dissipation (liquid-like) and at short timescales of high frequencies, a plateau of G' is higher than G", showing a dominant elastic behavior (solid-like). In contrast, $S_1T_2D_1$ displays parallel curves of G' and G" across the entire frequency range at 25 °C, with G" consistently higher than G' (Figure 3f). This behavior arises from the introduction of flexible chains that lower the Tg, enabling faster molecular chain mobility and thereby enhancing viscoelasticity with liquid-like dominance. Furthermore, temperature-dependent frequency sweeps of $S_1T_2D_1$ (Figure 3g) demonstrate a gradual increase in G' as temperature decreased, signifying a transition from viscous to elastic behavior. The relaxation time of $S_1T_2D_1$ is further prolonged when the temperature decreases from 5 °C to 0 °C, causing the intersection point of G' and G" to shift towards the low-frequency direction (it appears "ahead of schedule"). This phenomenon reflects suppressed thermal motion of molecular chains at lower temperatures, which restricts segmental mobility and reinforces elastic contributions. The mechanical properties of the $S_XT_YD_Z$ were also evaluated by dynamic mechanical analysis (DMA) test. As expected, with the increase of TA, the loss factor tanδ of $S_XT_YD_Z$ gradually increases and the $S_XT_YD_Z$ polymers tend to be more viscous (Figures 3h, S43, S44 and Table S13).[67] Considering the dynamic nature of the disulfide bonds and the viscosity of $S_1T_2D_1$, its self-healing behavior was performed at 40 °C using an optical microscope (Figure S45). As shown in Figure S46, the signals of sulfur radicals become stronger, due to the heat accelerates the generation of sulfur radicals. Under heating conditions, the mobility of polymer chains increases more rapidly and the rate of disulfide bond exchange increases, thereby enabling complete self-healing within 3~4 hours.[68, 69] In summary, this TA-initiated strategy not only successfully overcomes the processing difficulties in inverse vulcanization polymer (for example S_1D_1 polymer in this work), but also could greatly improve both mechanical properties and recyclability of $S_XT_YD_Z$.

3.6 Adhesion Properties of $S_XT_YD_Z$

Compared to oxygen-containing compounds, sulfur-containing compounds serve as "polar hydrophobic" hydrogen bonding motifs that exhibit fewer N-H protons of thiourea exchanges with water, thereby enabling them to develop robust underwater adhesives.[70] But for inverse vulcanization polymers, it is difficult to form effective interactions with substrates due to their the low polarity and poor cohesive strength, thereby limiting their application in adhesives.[71, 72] Considering that the synthesized $S_XT_YD_Z$ polymers have good toughness, and its side chains contain carboxyl groups, which can interact with polar groups on the substrate through hydrogen bonding.[73] Additionally, the hydrophobicity exhibited by the polysulfide chains and benzene ring structures in the $S_XT_YD_Z$ polymers backbone allows for the exclusion of interfacial water under humid environments.[74]

To evaluate the adhesive performance of $S_XT_YD_Z$ following TA modification, we conducted adhesion tests through a hot-melt method and lap shear tests with the tensile machine (Figure S47). We first established three groups of control experiments, including S_1T_1 (1.153 MPa), S_1D_1 (0.605 MPa), and T_1D_1 (0.127 MPa), all of which exhibited weak adhesive strength (Figure S48). Among three control groups, T_1D_1 shows stickiness and can easily form interfacial interactions with the substrate, while S_1D_1 exhibits brittleness with good cohesive strength compared to T_1D_1. However, the $S_XT_YD_Z$ polymers modified with TA appear to have remarkable adhesive properties (3.75 - 4.55 MPa) and adhesion energy (0.7-1.4 MJ m^{-2}) (Figure 4b). This can be attributed to the hydrogen bonding between the carboxyl groups and the mechanical topography of the polar substrate. Compared to the control groups, $S_XT_YD_Z$ polymers not only show increased cohesive strength but also enhance interfacial interactions, indicating that the TA plays a significant role in the interfacial interaction between the adhesive and the substrate.

Subsequently, we explored an in-depth investigation into the water contact angle, swelling resistance and cohesive strength of $S_XT_YD_Z$. We first conducted water contact angle experiments

View Article Online
DOI: 10.1039/D5PY00658A

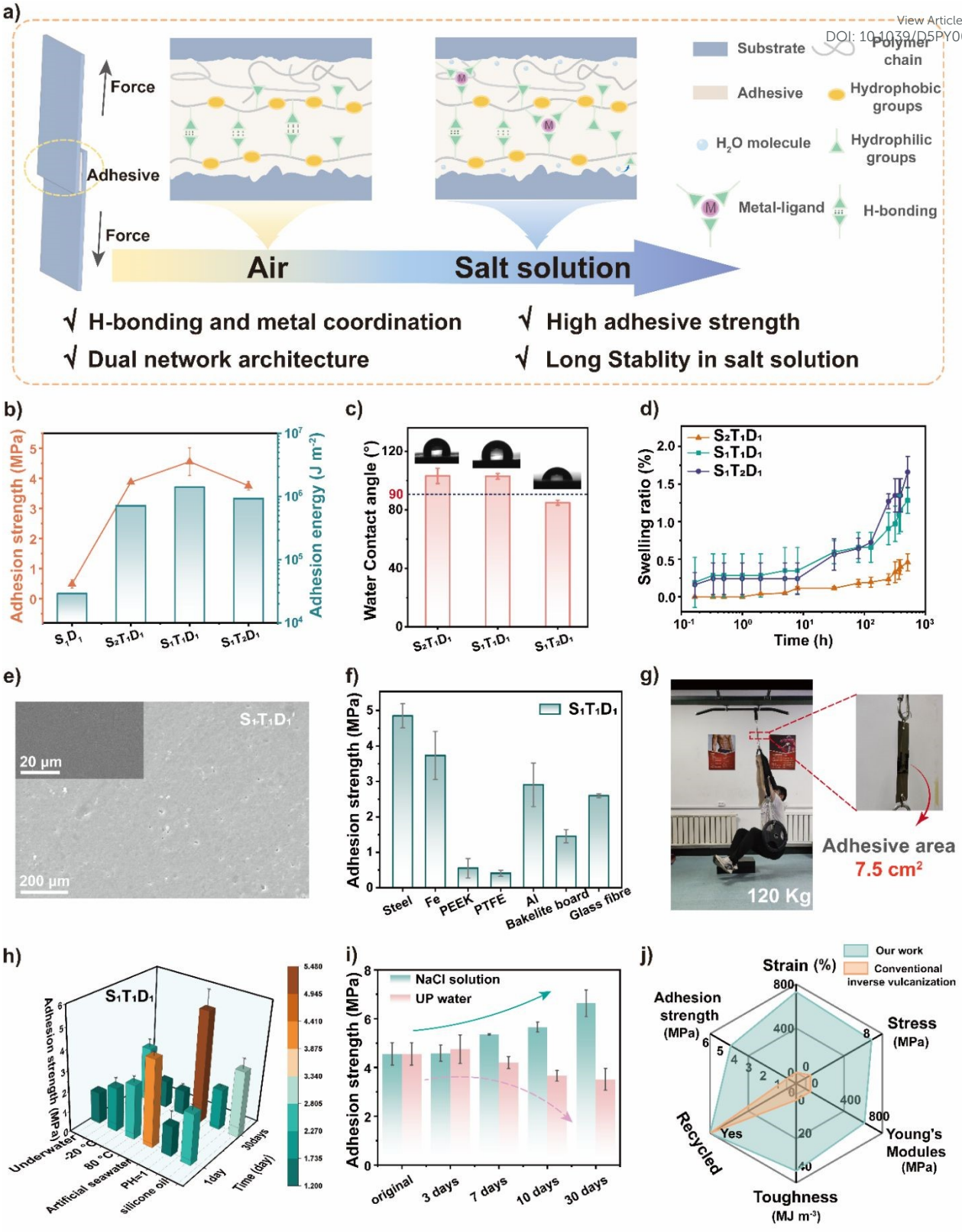

Figure 4 Adhesion Behavior of $S_XT_YD_Z$. a) Interaction mechanism of the $S_XT_YD_Z$ with the substrate. b) Adhesive strength of $S_XT_YD_Z$ and its control S_1D_1 under R.T. c) Water contact angle of $S_XT_YD_Z$. d) Swelling behavior of $S_XT_YD_Z$ in PU water at 25 °C. e) SEM image of $S_1T_1D_1$ following a 21-day immersion. f) Adhesive strength under different substrates of $S_1T_1D_1$. g) Picture illustrating two steel base plates bonded, capable of withstanding a load of 120 kg (approximately 1176 N). h) Adhesive strength measurements of $S_1T_1D_1$ in different environments after one day and thirty days. i) Adhesive strength measurements of $S_1T_1D_1$ immersed in saturated NaCl solution and UP water at different time intervals. j) Radar chart depicts a comparison of the mechanical and adhesive properties between the conventional inverse vulcanization polymer and $S_1T_1D_1$ of our work.

on the $S_XT_YD_Z$ polymer. The water contact angle test reveals that both $S_1T_1D_1$ and $S_2T_1D_1$ are hydrophobic, which is attributed to the hydrophobic groups of polysulfide chains and benzene ring structures present in their backbones (Figure 4c). After

immersing $S_XT_YD_Z$ polymer in UP water for 21 days, we found that the maximum swelling ratio reached only 1.5% of the original weight of the $S_XT_YD_Z$ polymers (Figure 4d). Meanwhile, SEM tests were conducted to characterize the surface condition of the $S_XT_YD_Z$, after immersion in water for 21 days. It was found that the surface of $S_1T_2D_1$ had already cracked, while the surfaces of $S_2T_1D_1$ and $S_1T_1D_1$ remained smooth (Figure S49). This indicates that a high content of hydrophobic structures such as sulfur chains and benzene rings in $S_XT_YD_Z$ polymers can more effectively repel water and provide superior cohesive strength.

Besides, the SEM analysis was also conducted to characterize the morphology of the $S_XT_YD_Z$ after adhesion failure and found that the surfaces of $S_2T_1D_1$ and $S_1T_2D_1$ exhibited protrusions (Figures 4e and S50). These protrusions may be produced by the insufficient interaction between the adhesion layer and the interface when subjected to external forces, whereas $S_1T_1D_1$ does not show any protrusions. Therefore, we selected $S_1T_1D_1$, which exhibits excellent hydrophobicity and high bond strength, for the subsequent bonding test on different substrates and harsh environments. We conducted lap shear tests on $S_1T_1D_1$ with different substrate materials and evaluated its load-bearing capacity on stainless steel samples with a 7.5 cm^2 adhesive area (Figures 4f and 4g). It can be able to bear a weight of 120 kg, demonstrating excellent load-bearing performance.

Long-term resistance to harsh environments is an important indicator for evaluating the adhesive performance. Therefore, we conducted adhesion tests on the $S_1T_1D_1$ under various harsh conditions, including temperatures of -20 °C, -80 °C, artificial seawater as well as strong acid environments (Table S15). We found that $S_1T_1D_1$ still maintained good adhesive properties (Figure 4h). Notably, after 30 days of immersion in artificial seawater, the bond strength shows a significant enhancement from 4.24±0.19 MPa to 5.46±0.85 MPa. Owing to the strong adhesive strength of $S_1T_1D_1$, it was not possible to effectively test the glass substrate. Additionally, we placed $S_1T_1D_1$ in saturated saltwater for an underwater load-bearing experiment. The $S_1T_1D_1$ adhesive has been bearing weight for more than 130 days without any fracture (Figure S51). Considering the bonding performance enhancement of $S_1T_1D_1$ in artificial seawater, we speculate that perhaps the carboxyl group of the side chain of $S_1T_1D_1$ is coordinated with metal ions for enhancing the cohesive strength of $S_1T_1D_1$ polymer and its interfacial interaction with the substrate, thus maintaining the long-term stability of underwater load-bearing in salt solution. To verify our hypothesis, we designed a control experiment by immersing $S_1T_1D_1$ in both UP water and saturated NaCl solution to test its adhesive strength at different time intervals. As shown in Figure 4i, the adhesive strength of the $S_1T_1D_1$ immersed in UP water decreases rather than increases, whereas a significant increase is observed in the saturated NaCl solution. This observation is that $S_1T_1D_1$ may achieve metal coordination enhancement in salt solutions, thereby realizing long-term stability in saline environments. Ultimately, we compiled recent studies on the tensile and adhesion strength of polysulfides and compared the conventional inverse vulcanization S_1D_1 control with our work (Figure 4j and Table S17), and $S_XT_YD_Z$ polymers of our work show outstanding adhesive and mechanical properties. We believe that the $S_XT_YD_Z$ polymers can serve as an advanced adhesive material in the field of sulfur-containing polymers.

Conclusions

In summary, by modifying conventional inverse vulcanization S_1D_1 with TA, we achieved thermoplastic polymers ($S_XT_YD_Z$) with short sulfur rank and improved mechanical properties for humid adhesion. TA can initiate the ROP of S_8 at 120 °C and insert into the polysulfide chain, forming the STA chain with alternating arrangement of PTA and the S atoms, in contrast to the chaotic, long and disordered sulfur chain in S_1D_1. Compared to the control S_1D_1, brittle and difficultly polymer, the $S_2T_1D_1$ polymer exhibits good mechanical properties (8.5 MPa) and enhanced recyclability (8.48 ~ 11.64 MPa). Crucially, the carboxyl groups confer exceptional humid adhesion stability in saline environments for 130 days via metal ion coordination, enhancing cohesive strength. The formulation of these polymers paves the way for the efficient and clean utilization of elemental sulfur, driving the sustainable progression of sulfur-containing polymer development.

Author contributions

Tongye Zhang: Methodology; Formal analysis; Data curation; Writing-original draft. Zhiyue Fang: Formal analysis. Shifang Luan: Project administration; Funding acquisition. Lei Wang: Writing-review & editing; Supervision; Conceptualization. Hengchong Shi: Conceptualization; Project administration; Funding acquisition.

Conflicts of interest

The authors declare that they have no conflicts of interest.

Data availability

The data supporting this article have been included as part of the ESI. †

Acknowledgements

This work is supported by the National Natural Science Foundation of China (Grant No. 52373049), Scientific and Technological Development Program of Jilin Province (Grant No. 20240305045YY), and the Chinese Academy of Sciences-Wego Group Hightech Research & Development Program. The authors would like to thank Xinghong Zhang of the Department of Polymer Science and Engineering of Zhejiang University for helpful discussions on topics related to this work. The authors are also very grateful to Donghua Xu of the State Key Laboratory of Polymer Science and Technology, Changchun Institute of Applied Chemistry, Chinese Academy of Sciences. The authors extend their gratitude to the Shiyanjia Lab (www.shiyanjia.com)

View Article Online
DOI: 10.1039/D5PY00658A

for providing invaluable assistance with the XPS and EPR analysis.

Notes and references

1 J. Lim, J. Pyun and K. Char, Angew. Chem., 2015, **127,** 3298-3308.
2 S. T. Ota and G. L. Richmond, J. Am. Chem. Soc., 2011, **133,** 7497-7508.
3 Y. Zhang, R. S. Glass, K. Char and J. Pyun, Polym. Chem., 2019, **10,** 4078-4105.
4 J. Lim, J. Pyun and K. Char, Angew. Chem. Int. Ed., 2015, **54,** 3249-3258.
5 J. J. Griebel, R. S. Glass, K. Char and J. Pyun, Prog. Polym. Sci., 2016, **58,** 90-125.
6 S. Luo, N. Wang, Y. Pan, B. Zheng, F. Li and S. Dong, Small, 2024, **20,** e2310839.
7 S. Penck, M. Cypryk, J. Pretula, K. Kaluzynski and P. Lewinski, Prog. Polym. Sci., 2024, **152,** 101818.
8 M. J. H. Worthington, R. L. Kucera and J. M. Chalker, Green Chem., 2017, **19,** 2748-2761.
9 W. J. Chung, J. J. Griebel, E. T. Kim, H. Yoon, A. G. Simmonds, H. J. Ji, P. T. Dirlam, R. S. Glass, J. J. Wie, N. A. Nguyen, B. W. Guralnick, J. Park, Á. Somogyi, P. Theato, M. E. Mackay, Y.-E. Sung, K. Char and J. Pyun, Nat. Chem., 2013, **5,** 518-524.
10 M. Lee, Y. Oh, J. Yu, S. G. Jang, H. Yeo, J.-J. Park and N.-H. You, Nat. Commun., 2023, **14,** 2866.
11 J. J. Griebel, S. Namnabat, E. T. Kim, R. Himmelhuber, D. H. Moronta, W. J. Chung, A. G. Simmonds, K. J. Kim, J. van der Laan, N. A. Nguyen, E. L. Dereniak, M. E. Mackay, K. Char, R. S. Glass, R. A. Norwood and J. Pyun, Adv. Mater., 2014, **26,** 3014-3018.
12 J. J. Griebel, S. Namnabat, E. T. Kim, R. Himmelhuber, D. H. Moronta, W. J. Chung, A. G. Simmonds, K.-J. Kim, J. van der Laan, N. A. Nguyen, E. L. Dereniak, M. E. Mackay, K. Char, R. S. Glass, R. A. Norwood and J. Pyun, Adv. Mater., 2014, **26,** 3014-3018.
13 J. Zhou, M. L. Holekevi Chandrappa, S. Tan, S. Wang, C. Wu, H. Nguyen, C. Wang, H. Liu, S. Yu, Q. R. S. Miller, G. Hyun, J. Holoubek, J. Hong, Y. Xiao, C. Soulen, Z. Fan, E. E. Fullerton, C. J. Brooks, C. Wang, R. J. Clément, Y. Yao, E. Hu, S. P. Ong and P. Liu, Nature, 2024, **627,** 301-305.
14 W. Cao, F. Dai, R. Hu and B. Z. Tang, J. Am. Chem. Soc., 2019, **142,** 978-986.
15 T. Tian, R. Hu and B. Z. Tang, J. Am. Chem. Soc., 2018, **140,** 6156-6163.
16 Y. Onose, Y. Ito, J. Kuwabara and T. Kanbara, Polym. Chem., 2022, **13,** 5486-5493.
17 K. Orme, A. H. Fistrovich and C. L. Jenkins, Macromolecules, 2020, **53,** 9353-9361.
18 J. Jia, J. Liu, Z.-Q. Wang, T. Liu, P. Yan, X.-Q. Gong, C. Zhao, L. Chen, C. Miao, W. Zhao, S. Cai, X.-C. Wang, A. I. Cooper, X. Wu, T. Hasell and Z.-J. Quan, Nat. Chem., 2022, **14,** 1249-1257.
19 P. Yan, W. Zhao, F. McBride, D. Cai, J. Dale, V. Hanna and T. Hasell, Nat. Commun., 2022, **13,** 4824.
20 H. Yang, J. Huang, Y. Song, H. Yao, W. Huang, X. Xue, L. Jiang, Q. Jiang, B. Jiang and G. Zhang, J. Am. Chem. Soc., 2023, **145,** 14539-14547.
21 D. Wang, Z. Tang, Y. Liu and B. Guo, Green Chem., 2020, **22,** 7337-7342.
22 J. Y. Chao, T. J. Yue, B. H. Ren, G. G. Gu, X. B. Lu and W. M. Ren, Angew. Chem. Int. Ed., 2022, **61,** e202115950.
23 J. M. M. Pople, T. P. Nicholls, L. N. Pham, W. M. Bloch, L. S. Lisboa, M. V. Perkins, C. T. Gibson, M. L. Coote, Z. Jia and J. M. Chalker, J. Am. Chem. Soc., 2023, DOI: 10.1021/jacs.3c03239.
24 J. Zhang, Q. Zang, F. Yang, H. Zhang, J. Z. Sun and B. Z. Tang, J. Am. Chem. Soc., 2021, **143,** 3944-3950.
25 W. Cao, F. Dai, R. Hu and B. Z. Tang, J. Am. Chem. Soc., 2020, **142,** 978-986.
26 D. H. Kim, W. Jang, K. Choi, J. S. Choi, J. Pyun, J. Lim, K. Char and S. G. Im, Sci. Adv., 2020, **6,** eabb5320.
27 J. Kuwabara, K. Oi, M. M. Watanabe, T. Fukuda and T. Kanbara, ACS Appl. Polym. Mater., 2020, **2,** 5173-5178.
28 L. J. Dodd, Ö. Omar, X. Wu and T. Hasell, ACS Catal., 2021, **11,** 4441-4455.
29 K.-S. Kang, A. Phan, C. Olikagu, T. Lee, D. A. Loy, M. Kwon, H.-j. Paik, S. J. Hong, J. Bang, W. O. Parker Jr, M. Sciarra, A. R. de Angelis and J. Pyun, Angew. Chem. Int. Ed., 2021, **60,** 22900-22907.
30 B.-J. Lee, C. Zhao, J.-H. Yu, T.-H. Kang, H.-Y. Park, J. Kang, Y. Jung, X. Liu, T. Li, W. Xu, X.-B. Zuo, G.-L. Xu, K. Amine and J.-S. Yu, Nat. Commun., 2022, **13,** 4629.
31 D. Wang, Z. Tang, Z. Wang, L. Zhang and B. Guo, Polym. Chem., 2022, **13,** 485-491.
32 D. Wang, Z. Tang, S. Fang, S. Wu, H. Zeng, A. Wang and B. Guo, Carbon, 2021, **184,** 409-417.
33 Y. Huang, Y. Liu, G. Si and C. Tan, ACS Sustainable Chem. Eng., 2024, **12,** 2212-2224.
34 V. S. Wadi, K. K. Jena, K. Halique, Brigita Rožič, L. Cmok, V. Tzitzios and S. M. Alhassan, Sci. Rep., 2020, **10.**
35 J. Bao, K. P. Martin, E. Cho, K.-S. Kang, R. S. Glass, V. Coropceanu, J.-L. Bredas, W. O. N. Parker, J. T. Njardarson and J. Pyun, J. Am. Chem. Soc., 2023, **145,** 12386-12397.
36 A. Eisenberg and A. V. Tobolsky, J. Polym Sci., 2003, **46,** 19-28.
37 A. V. Tobolsky, Journal of Polymer Science Part C: Polymer Symposia, 2007, **12,** 71-78.
38 Q. Laurent, N. Sakai and S. Matile, Helv. Chim. Acta, 2019, **102,** e1800209.
39 A. D. Clauss, S. F. Nelsen, M. Ayoub, J. W. Moore, C. R. Landis and F. Weinhold, Chem. Educ. Res. Pract., 2014, **15,** 417-434.
40 Z. Wang, D. Chen, H. Wang, S. Bao, L. Lang, C. Cui, H. Song, J. Yang and W. Liu, Adv. Mater., 2024, **36,** 2404297.
41 K. R. Albanese, P. T. Morris, J. Read de Alaniz, C. M. Bates and C. J. Hawker, J. Am. Chem. Soc., 2023, **145,** 22728-22734.
42 K.-X. Hou, S.-P. Zhao, D.-P. Wang, P.-C. Zhao, C.-H. Li and J.-L. Zuo, Adv. Funct. Mater., 2021, **31,** 2107006.
43 Y. Deng, Q. Zhang, B. L. Feringa, H. Tian and D. H. Qu, Angew. Chem. Int. Ed., 2020, **59,** 5278-5283.
44 C. Chen, X. Yang, S.-j. Li, C. Zhang, Y.-n. Ma, Y.-x. Ma, P. Gao, S.-z. Gao and X.-j. Huang, Green Chem., 2021, **23,** 1794-1804.
45 Q. Zhang, D.-H. Qu, B. L. Feringa and H. Tian, J. Am. Chem. Soc., 2022, **144,** 2022-2033.
46 L. Packer, E. H. Witt and H. J. Tritschler, Free Radical Biol. Med., 1995, **19,** 227-250.
47 J. Huang, A. A. Wróblewska, J. Steinkoenig, S. Maes and F. E. Du Prez, Macromolecules, 2021, **54,** 4658-4668.
48 Z. Fang, L. Wang, C. Liang, J. Qiu, T. Zhang, D. Xu, D. Qi, S. Luan and H. Shi, Adv. Funct. Mater., 2025, **35,** 2418583.
49 A. Khan, R. R. Kisannagar, C. Gouda, D. Gupta and H.-C. Lin, J. Mater. Chem. A, 2020, **8,** 19954-19964.
50 S. Pal, J. Shin, K. DeFrates, M. Arslan, K. Dale, H. Chen, D. Ramirez and P. B. Messersmith, Science, 2024, **385,** 877-883.
51 P. T. Morris, K. Watanabe, K. R. Albanese, G. T. Kent, R. Gupta, M. Gerst, J. Read de Alaniz, C. J. Hawker and C. M. Bates, J. Am. Chem. Soc., 2024, **146,** 30662-30667.
52 X. Wei, X. Zhang, T. Chen, J. Huang, T. Li, X. Zhang, S. Wang and W. Dong, ACS Macro Lett., 2024, **13,** 1112-1118.
53 L. Wang, K. Yue, Q. Qiao, Z. Zhao, Y. Xu, L. Pan, Y. Liu, H. Li and B. Zhu, Adv. Energy Mater., 2024, **15,** 2402617.
54 Z. Sun, Q. Ou, C. Dong, J. Zhou, H. Hu, C. Li and Z. Huang, Exploration, 2024, **4,** 20220167.
55 X.-Y. Hao, B. Yu, L. Li, H. Ju, M. Tian and P.-F. Cao, Macromolecules, 2024, **57,** 5063-5072.
56 L. J. Dodd, RSC Appl. Polym., 2025, **3,** 10-42.

View Article Online
DOI: 10.1039/D5PY00658A

57 Y. Deng, Z. Huang, B. L. Feringa, H. Tian, Q. Zhang and D.-H. Qu, Nat. Commun., 2024, **15,** 3855.
58 S. P. O. Danielsen, H. K. Beech, S. Wang, B. M. El-Zaatari, X. Wang, L. Sapir, T. Ouchi, Z. Wang, P. N. Johnson, Y. Hu, D. J. Lundberg, G. Stoychev, S. L. Craig, J. A. Johnson, J. A. Kalow, B. D. Olsen and M. Rubinstein, Chem. Rev., 2021, **121,** 5042-5092.
59 J. Zhang, M. Wang, X. Yao, J. Liu and B. Yan, ACS Appl. Mater. Interfaces, 2024, **16,** 54685-54692.
60 M. Huang, L. Liu, W. Guo, L. Cui, G. Gao, Q. Zhang and X. Liu, Adv. Funct. Mater., 2025, **35,** 2413542.
61 S. Yu, Z. Tang, D. Wang, B. Guo and L. Zhang, Macromolecules, 2024, **57,** 10120-10129.
62 J. J. Dale, S. Petcher and T. Hasell, ACS Appl. Polym. Mater., 2022, 4, 3169-3173.
63 J. J. Dale, J. Stanley, R. A. Dop, G. Chronowska-Bojczuk, A. J. Fielding, D. R. Neill and T. Hasell, Eur. Polym. J., 2023, **195,** 112198.
64 C. W. H. Rajawasam, O. J. Dodo, M. A. S. N. Weerasinghe, I. O. Raji, S. V. Wanasinghe, D. Konkolewicz and N. De Alwis Watuthanthrige, Polym. Chem., 2024, **15,** 219-247.
65 M. A. S. N. Weerasinghe, O. J. Dodo, C. W. H. Rajawasam, I. O. Raji, S. V. Wanasinghe, D. Konkolewicz and N. De Alwis Watuthanthrige, Polym. Chem., 2023, **14**, 4503-4514.
66 P. Yan, W. Zhao, S. J. Tonkin, J. M. Chalker, T. L. Schiller and T. Hasell, Chem. Mater., 2022, **34,** 1167-1178.
67 J. J. Griebel, N. A. Nguyen, S. Namnabat, L. E. Anderson, R. S. Glass, R. A. Norwood, M. E. Mackay, K. Char and J. Pyun, ACS Macro Lett., 2015, **4,** 862-866.
68 C. Cui, F. Wang, X. Chen, T. Xu, Z. Li, K. Chen, Y. Guo, Y. Cheng, Z. Ge and Y. Zhang, Adv. Funct. Mater., 2024, **34,** 2315469.
69 X. Xue, C. Li, X. Yu, K. Chenchai, X. Zhang, X. Zhang, G. Zhang and D. Zhang, Angew. Chem. Int. Ed., 2025, **64,** e202425172.
70 K. Kikkawa, Y. Sumiya, K. Okazawa, K. Yoshizawa, Y. Itoh and T. Aida, J. Am. Chem. Soc., 2024, **146,** 21168-21175.
71 H. Huang, S. Zheng, J. Luo, L. Gao, Y. Fang, Z. Zhang, J. Dong and N. Hadjichristidis, Angew. Chem. Int. Ed., 2024, **63,** e202318919.
72 Y. Jin, Z. Wang, C. Hu, J. Wang, K. Yan, J. He, Z. Wang, Z. Wang and L. Yuan, Green Chem., 2023, **25,** 1157-1168.
73 C. Cui, L. Mei, D. Wang, P. Jia, Q. Zhou and W. Liu, Nat. Commun., 2023, **14,** 7707.
74 B. Cheng, J. Yu, T. Arisawa, K. Hayashi, J. J. Richardson, Y. Shibuta and H. Ejima, Nat. Commun., 2022, **13,** 1892.

The data supporting this article have been included as part of the ESI. †

View Article Online
DOI: 10.1039/D5PY00658A